INTERNATIONAL JOURNAL FOR NUMERICAL AND ANALYTICAL METHODS IN GEOMECHANICS, VOL. 20, 549–569 (1996)

A PLANE MODEL FOR THE STRESS FIELD AROUND AN INCLINED, CASED AND CEMENTED WELLBORE

C. ATKINSON

Department of Mathematics, Imperial College of Science, Technology and Medicine, 180 Queen's Gate, London SW7 2BZ, U.K.

AND

D. A. EFTAXIOPOULOS

Department of Interpretation and Geomechanics, Schlumberger Cambridge Research, High Cross, Madingley Road, Cambridge CB3 0EL, U.K.

SUMMARY

In-plane and out-of-plane analyses for the stress field around an internally pressurized, cased, cemented and remotely loaded circular hole have been developed in this report. Taking into account the well-known solution for a pressurized circular hole in an infinite medium, we have effected appropriate complex potentials for the steel ring and the cement annulus, such that continuity of stresses and displacements is maintained along the steel/cement and cement/rock interfaces and prescribed pressure is imposed along the open hole. Results indicate that the plane of the maximum tangential stress may rotate 90°, between the steel/cement and the cement/rock interfaces. A quantitative justification for the occurrence of such a rotation is presented, by considering the hole, the steel and the cement layers as a single 'equivalent' inclusion, bonded on the rock matrix.

KEY WORDS: inclined wellbore; stress field; plane model

0. INTRODUCTION

Drilling of deviated wells is important in the oil recovery industry. Inclined wellbores are of great importance offshore, in the treatment of thin reservoirs, in cases of anisotropic formations where the permeability varies in different directions, in producing from naturally fractured reservoirs and in delaying the breakthrough of water or gas coning.

Steel casing and cementing of the borehole enhance its stability, especially when weak formation are dealt with.

The knowledge of the stress field around a wellbore is crucial is hydraulic fracturing, since this can elucidate, to some extent, the fracture initiation and propagation processes. Inclination of the well results in the development of Mode III fracture due to out-of-plane shear stresses, generated due to the earth's remote stresses. The presence of the casing tube and the cement annulus often leads to discontinuities of the tangential stress, which may affect the fracture aperture quite severely.

Carvalho[1] has analysed open hole deviated wells, in generalized plain strain conditions, in order to investigate fracture initiation and borehole stability, Carter *et al.*[2] have used FRANC2D — a fracture analysis code — to examine the effect of casing and cement on fracture propagation. They have obtained results for the tangential stress, around the wellbore and close to the hole edge and at the steel–cement and the cement–rock interfaces. In this study, a plane model for the

CCC 0363–9061/96/080549–21

Received 27 March 1995
Revised 11 December 1995

stress field around an inclined, cased and cemented wellbore has been developed. First, the plane problem of an internally pressurized circular hole, surrounded by two rings of different materials and remotely loaded by principal in-plane stresses, is solved. Continuity of stress and displacements is assumed along the interfaces, i.e. the bond is considered as perfect. Secondly, the anti-plane problem, with the same geometry as the above stated in-plane problem, but with anti-plane stresses induced at infinity, is tackled. For both cases, the theory of complex potentials, as developed by Muskhelishvili,[3] is implemented.

Assuming the functional form of the complex potentials for the rock as known, new ones are developed for the cement and steel rings, via the satisfaction of the continuity boundary conditions along the interfaces. Appropriate coefficients are finally defined by enforcing the normal stress to be equal to the prescribed internal pressure, along the open hole edge. All three potential functions, i.e for the rock, the cement and the steel, are expressed in terms of those coefficients and thus uniquely determined.

In a particular example that we have treated, where the modulus of elasticity of the rock is much smaller than that of the cement, numerical results indicated that there is a 90° rotation of the plane of maximum (least compressive) tangential stress, between the steel/cement and the cement/rock interfaces. Such a rotation was not observed when the Young's modulus of the rock was sufficiently larger than that of the cement. In order to check the validity of these results, a model is considered whereby the hole, the steel and the cement layers are replaced by an 'equivalent' inclusion, with shear modulus related to the individual moduli of the two layers and the hole, through the average of the areas that they occupy. Results from the 'equivalent' inclusion problem confirmed the rotation of the plane of the maximum tangential stress at 90° and a rule of thumb for its prediction was effected, via a relation between the material moduli of the rock, the cement and the steel and the radii of the open hole and the rock/cement and cement/steel interfaces.

For both the hoop stress and the anti-plane tangential stress, a reverse of their decreasing (in absolute value) trend occurred, while moving from the steel/cement to the cement/rock interfaces, when the rock elasticity modulus become sufficiently larger than that of the cement.

1. THE IN-PLANE STRESS FIELD, DUE TO A CASED, CEMENTED, INTERNALLY PRESSURIZED CIRCULAR HOLE, REMOTELY LOADED BY PRINCIPAL COMPRESSIVE STRESSES

A Cartesian co-ordinate system $O(x_1, x_2, x_3)$ and cylindrical–polar co-ordinate system $O(r, \theta, x_3)$ are introduced (Figure 1). The x_3 axis is perpendicular to the $x_1 - x_2$ plane.

A circular hole of radius R_1, centred at O and internally pressurized by uniform pressure p, is cased by a steel ring of width $R_2 - R_1$ and cemented by an annulus of width $R_3 - R_2$. The principal stresses at infinity are σ_1 and σ_2 and are parallel to the x_1 and x_2 axes respectively. Superscripts (1), (2), (3) refer to steel, cement and rock respectively. Compression is denoted by assigning negative arithmetic values to the stress and pressure variables.

Stresses and displacements for plane linear elasticity problems, with reference to a polar co-ordinate system $O(r, \theta)$, are given in Reference 3 in terms of potentials $\Phi(z)$ and $\Psi(z)$ of the complex variable $z = x_1 + ix_2$, as

$$\sigma_{rr} + \sigma_{\theta\theta} = 2[\Phi(z) + \overline{\Phi(z)}] \tag{1}$$

$$\sigma_{\theta\theta} - \sigma_{rr} + 2i\sigma_{r\theta} = 2\frac{z}{\bar{z}}[\bar{z}\Phi'(z) + \Psi(z)] \tag{2}$$

$$2\mu e^{i\theta}(u_r + iu_\theta) = \kappa\phi(z) - z\overline{\Phi(z)} - \overline{\psi(z)} + \text{constant} \tag{3}$$

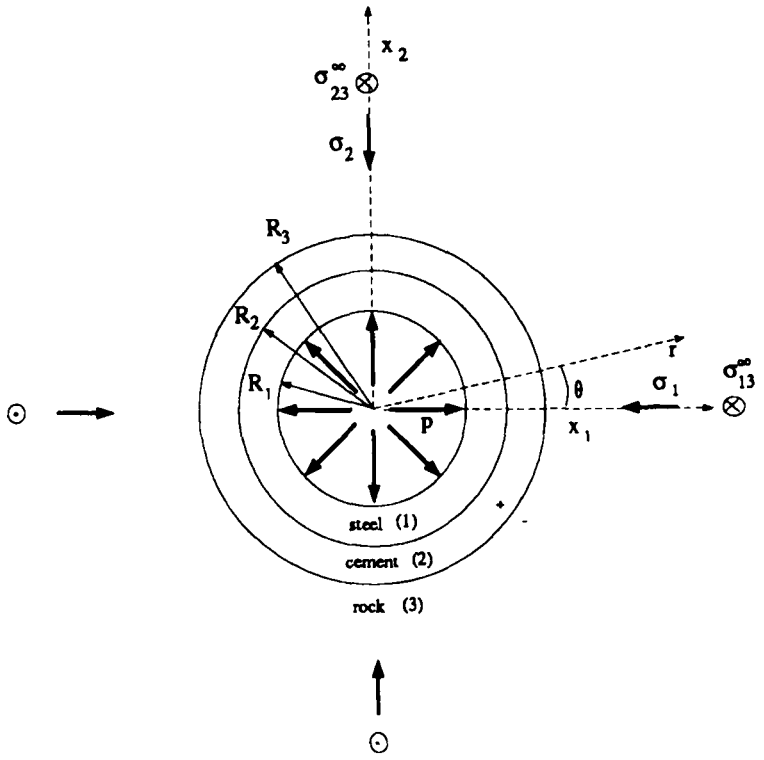

Figure 1. A plane cross-section of an inclined, cased and cemented wellbore, remotely loaded by in-plane and anti-plane stresses

where $\phi(z) = \Phi'(z)$, $\psi(z) = \Psi'(z)$ are the first-order derivatives of $\Phi(z)$ and $\Psi(z)$ respectively, μ is the shear modulus, $\kappa = 3 - 4\nu$ for plain strain and ν is Poisson's ratio. The prime denotes first-order derivatives with respect to z.

The boundary conditions to be satisfied are the following:

For $|z| \to \infty$

$$\sigma_{xx}^{(3)} = \sigma_1 \tag{4}$$

$$\sigma_{yy}^{(3)} = \sigma_2 \tag{5}$$

For $|z| = R_3$

$$\sigma_{rr}^{(2)} + i\sigma_{r\theta}^{(2)} = \sigma_{rr}^{(3)} + i\sigma_{r\theta}^{(3)} \tag{6}$$

$$u_r^{(2)} + iu_\theta^{(2)} = u_r^{(3)} + iu_\theta^{(3)} \tag{7}$$

For $|z| = R_2$

$$\sigma_{rr}^{(1)} + i\sigma_{r\theta}^{(1)} = \sigma_{rr}^{(2)} + i\sigma_{r\theta}^{(2)} \tag{8}$$

$$u_r^{(1)} + iu_\theta^{(1)} = u_r^{(2)} + iu_\theta^{(2)} \tag{9}$$

For $|z| = R_1$

$$\sigma_{rr}^{(1)} + i\sigma_{r\theta}^{(1)} = p \tag{10}$$

Muskhelishvili[3] has derived the solution for the first fundamental problem for the circular hole in an infinite medium. Taking that solution into account, we initially chose the complex potentials for the rock as

$$\Phi^{(3)}(z) = A^{(3)} + \frac{B^{(3)}}{z^2} \tag{11}$$

$$\Psi^{(3)}(z) = D^{(3)} + \frac{F^{(3)}}{z^2} + \frac{G^{(3)}}{z^4} \tag{12}$$

where $A^{(3)}$, $B^{(3)}$, $F^{(3)}$, $G^{(3)}$ are constants to be determined such that the boundary conditions (4)–(10) are satisfied. Expressing (4), (5) via (1), (2) in terms of (11) and (12) and letting $|z| \to \infty$, we immediately obtain

$$A^{(3)} = \frac{\sigma_1 + \sigma_2}{4} \tag{13}$$

$$D^{(3)} = \frac{\sigma_2 - \sigma_1}{2} \tag{14}$$

Subtracting (2) from (1) gives

$$\sigma_{rr} + i\sigma_{r\theta} = \Phi(z) + \overline{\Phi(z)} - \bar{z}\overline{\Phi'(z)} - \frac{\bar{z}}{z}\overline{\Psi(z)} \tag{15}$$

Further, by differentiating (3) with respect to θ we can extract

$$2\mu \frac{\partial}{\partial \theta}\left[e^{i\theta}(u_r + iu_\theta)\right] = iz\left[\kappa\Phi(z) - \overline{\Phi(z)} + \bar{z}\overline{\Phi'(z)} + \frac{\bar{z}}{z}\overline{\psi(z)}\right] \tag{16}$$

Taking into account the analysis in Reference 4, since $\bar{z} = R_3^2/z$ along $r = R_3$, we make the substitution

$$\Omega\left(\frac{R_3^2}{\bar{z}}\right) = \overline{\Phi(z)} - \bar{z}\overline{\Phi'(z)} - \frac{\bar{z}^2}{R_3^2}\overline{\Psi(z)} \tag{17}$$

in (15), (16) and we can finally express the boundary conditions, in terms of potentials $\Phi(z)$ and $\Omega(z)$, as follows:

For $t = R_3 e^{i\theta}$

$$[\Phi(t) - \Omega(t)]^+ = [\Phi(t) - \Omega(t)]^- \tag{18}$$

$$\frac{1}{\mu^{(2)}}[\kappa^{(2)}\Phi^+(t) - \Omega^-(t)] = \frac{1}{\mu^{(3)}}[\kappa^{(3)}\Phi^-(t) - \Omega^+(t)] \tag{19}$$

For $t = R_2 e^{i\theta}$

$$[\Phi(t) - \Omega(t)]^+ = [\Phi(t) - \Omega(t)]^- \tag{20}$$

$$\frac{1}{\mu^{(1)}}[\kappa^{(1)}\Phi^+(t) - \Omega^-(t)] = \frac{1}{\mu^{(2)}}[\kappa^{(2)}\Phi^-(t) - \Omega^+(t)] \tag{21}$$

For $t = R_1 e^{i\theta}$

$$\Phi^-(t) + \Omega^+(t) = p \tag{22}$$

Note that superscripts (+) and (−) refer to the inner and outer regions of a circular boundary. The algebraic expressions of the constants that are not defined in this section can be found in Appendix I.

From (11), (12) and (17) it can be shown that

$$\Omega^{(3)}(z_3) = H^{(3)} + \frac{I^{(3)}}{z_3^2} + J^{(3)} z_3^2 \tag{23}$$

where $z_j = R_j e^{i\theta}$ for $j = 1, 2, 3$.

Solving the system (18), (19) with respect to $\Phi^{(2)}(z_3)$, $\Omega^{(2)}(z_3)$, we get

$$\Phi^{(2)}(z_3) = Y_1^{(2,3)} \Phi^{(3)}(z_3) + Y_2^{(2,3)} \Omega^{(3)}(z_3) \tag{24}$$

$$\Omega^{(2)}(z_3) = Y_3^{(2,3)} \Phi^{(3)}(z_3) + Y_4^{(2,3)} \Omega^{(3)}(z_3) \tag{25}$$

and after replacing $\Phi^{(3)}(z_3)$ and $\Omega^{(3)}(z_3)$ using (11) and (23), (24) and (25) turn

$$\Phi^{(2)}(z_3) = A^{(2)} + \frac{B^{(2)}}{z_3^2} + C^{(2)} z_3^2 \tag{26}$$

$$\Omega^{(2)}(z_3) = K^{(2)} + \frac{L^{(2)}}{z_3^2} + M^{(2)} z_3^2 \tag{27}$$

Hence, for the whole cement layer, superscripted $^{(2)}$, one finds

$$\Phi^{(2)}(z) = A^{(2)} + \frac{B^{(2)}}{z^2} + C^{(2)} z^2 \tag{28}$$

From (17)

$$\Psi(z) = \frac{\bar{z}}{z} \Phi(z) - \bar{z} \Phi'(z) - \frac{\bar{z}}{z} \overline{\Omega(z)} \tag{29}$$

follows and from (27) and (28) we get

$$\Psi^{(2)}(z) = D^{(2)} + \frac{F^{(2)}}{z^2} + \frac{G^{(2)}}{z^4} \tag{30}$$

We can also find $\Omega^{(2)}(z_2)$, form (17), (28) and (30), as

$$\Omega^{(2)}(z_2) = H^{(2)} + \frac{I^{(2)}}{z_2^2} + J^{(2)} z_2^2 \tag{31}$$

The process followed above for the cement annulus ($R_2 \leqslant r \leqslant R_3$) can be repeated for the steel casing ($R_1 \leqslant r \leqslant R_2$). Solving the system (20) and (21) with respect to $\Phi^{(1)}(z_2)$, $\Omega^{(1)}(z_2)$, we get

$$\Phi^{(1)}(z_2) = Y_1^{(1,2)} \Phi^{(2)}(z_2) + Y_2^{(1,2)} \Omega^{(2)}(z_2) \tag{32}$$

$$\Omega^{(1)}(z_2) = Y_3^{(1,2)} \Phi^{(2)}(z_2) + Y_4^{(1,2)} \Omega^{(2)}(z_2) \tag{33}$$

and after replacing $\Phi^{(2)}(z_2)$ and $\Omega^{(2)}(z_2)$ using (28) and (31), (32) gives

$$\Phi^{(1)}(z) = A^{(1)} + \frac{B^{(1)}}{z^2} + C^{(1)} z^2 \tag{34}$$

while for $z_2 = R_2 e^{i\theta}$, (33) turns out to be

$$\Omega^{(1)}(z_2) = K^{(1)} + \frac{L^{(1)}}{z_2^2} + M^{(1)} z_2^2 \tag{35}$$

From (29), (34) and (35) we obtain

$$\Psi^{(1)}(z) = D^{(1)} + \frac{F^{(1)}}{z^2} + \frac{G^{(1)}}{z^4} \tag{36}$$

and from (17), $\Omega^{(1)}(z_1)$ can be found as

$$\Omega^{(1)}(z_1) = H^{(1)} + \frac{I^{(1)}}{z_1^2} + J^{(1)} z_1^2 \tag{37}$$

From (34) and (37), (10) results in

$$A^{(1)} + H^{(1)} = p \tag{38}$$

$$B^{(1)} + I^{(1)} = 0 \tag{39}$$

$$C^{(1)} + J^{(1)} = 0 \tag{40}$$

so that (10) is satisfied for all θ along $r = R_1$.

Solution of (38)–(40) for $B^{(3)}$, $F^{(3)}$ and $G^{(3)}$ yields

$$F^{(3)} = \frac{p - Q_5 A^{(3)}}{Q_5} \tag{41}$$

$$B^{(3)} = \frac{D^{(3)}[-T_7 S_6 + S_7 T_6]}{T_5 S_6 - S_5 T_6} \tag{42}$$

$$G^{(3)} = \frac{D^{(3)}[-T_5 S_7 + S_5 T_7]}{T_5 S_6 - S_5 T_6} \tag{43}$$

Once $B^{(3)}$, $F^{(3)}$ and $G^{(3)}$ are known (see Appendix I), the complex potentials $\Phi^{(j)}(z)$ and $\Psi^{(j)}(z)$, with $j = 1, 2, 3$, for the steel casing, cement annulus and rock respectively, can be defined, from (34), (36), (28), (30), (11) and (12). Consequently, the stresses and displacements can be evaluated everywhere in the $x_1 - x_2$ plane.

2. THE ANTI-PLANE SHEAR STRESSES DUE TO A CASED, CEMENTED, INTERNALLY PRESSURIZED AND REMOTELY LOADED, CIRCULAR HOLE

Now, the anti-plane shear stresses at infinity are σ_{13}^{∞} and σ_{23}^{∞} (see Figure 1). Along the borehole circumference $\sigma_{r3} = 0$.

The stressed σ_{13}, σ_{23} and the displacement u_3 are now given in terms of a complex potential $f(z)$ as

$$\sigma_{13} - i\sigma_{23} = 2f'(z) \tag{44}$$

$$u_3 = \frac{1}{\mu}[f(z) + \overline{f(z)}] \tag{45}$$

The transformation formula that gives the stresses σ_{r3}, $\sigma_{\theta 3}$ with reference to the polar co-ordinate system $O(r, \theta, x_3)$ in terms of the stress σ_{13}, σ_{23}, is

$$\sigma_{r3} - i\sigma_{\theta 3} = e^{i\theta}[\sigma_{13} - i\sigma_{23}] \tag{46}$$

The boundary conditions of the problem are now the following:
For $|z| \to \infty$

$$\sigma_{13}^{(3)} - i\sigma_{23}^{(3)} = \sigma_{13}^{\infty} - i\sigma_{23}^{\infty} \tag{47}$$

For $|z| = R_3$

$$\sigma_{r3}^{(2)} = \sigma_{r3}^{(3)} \tag{48}$$

$$u_3^{(2)} = u_3^{(3)} \tag{49}$$

For $|z| = R_2$

$$\sigma_{r3}^{(1)} = \sigma_{r3}^{(2)} \tag{50}$$

$$u_3^{(1)} = u_3^{(2)} \tag{51}$$

For $|z| = R_1$

$$\sigma_{r3}^{(1)} = 0 \tag{52}$$

A method similar to the one followed in Section 1 we will be accomplished here. The algebraic expressions of the constants that are not defined in this section can be found in Appendix II.

Taking into account Reference 1, we initially choose

$$f'^{(3)}(z) = A^{(3)} + \frac{B^{(3)}}{z^2} \tag{53}$$

where the prime again denotes differentiation with respect to the complex variable z. $A^{(3)}$ can be immediately determined as

$$A^{(3)} = (\sigma_{13}^{\infty} - i\sigma_{23}^{\infty})/2 \tag{54}$$

from (46), (47), (53).

Differentiating (45) with respect to θ gives

$$\frac{\partial u_3}{\partial \theta} = \frac{iz}{\mu}\left[f'(z) - \frac{R^2}{z^2}\overline{f'}\left(\frac{R^2}{z}\right)\right] \tag{55}$$

Also from (44) and (46) we get

$$\sigma_{r3} = \frac{z}{R}f'(z) + \frac{R}{z}\overline{f'}\left(\frac{R^2}{z}\right) \tag{56}$$

From (48), (49), (55) and (56), it is derived that for $z_3 = R_3 e^{i\theta}$

$$f'^{(2)}(z_3) = Y_1^{(2,3)} f'^{(3)}(z_3) + Y_2^{(2,3)} \frac{R_3^2}{z_3^2}\overline{f'^{(3)}}\left(\frac{R_3^2}{z_3}\right) \tag{57}$$

$f'^{(2)}(z)$ can be chosen as the field function for the cement layer ($R_2 \leqslant r \leqslant R_3$) and taking into account (53) and (57), it can be expressed as

$$f'^{(2)}(z) = A^{(2)} + \frac{B^{(2)}}{z^2} \tag{58}$$

Repeating the same procedure along the steel–cement interface $z_2 = R_2 e^{i\theta}$, gives

$$f'^{(1)}(z) = A^{(1)} + \frac{B^{(1)}}{z^2} \tag{59}$$

with $A^{(1)}$ and $B^{(1)}$ given from (109) and (110).

Finally, from (52), (56) and (59), we get

$$B^{(1)} - R_1^2 A^{(1)} = 0 \tag{60}$$

and solving (60) for $B^{(3)}$ gives

$$B^{(3)} = \frac{Y_5 A^{(3)}}{Y_6} \tag{61}$$

Once $A^{(3)}$ and $B^{(3)}$ are determined, $f'^{(j)}(z)$ ($j = 1, 2, 3$) can also be evaluated at any point in the x_1–x_2 plane and subsequently the stresses can be calculated from (44), (46), (53), (54), (58), (109), (110), (59) and (61).

3. COMPARISON WITH FINITE ELEMENT RESULTS

Finite element results, for the in-plane stresses around a cased and cemented wellbore have been obtained in Reference 2. A plane borehole problem with $R_1 = 40$ mm, $R_2 = 50$ mm, $R_3 = 70$ mm, $\sigma_2 = -31$ MPa, $\sigma_1 = -48$ MPa, $p = -51{\cdot}7$ MPa, $E^{(1)} = 200$ GPa, $E^{(2)} = 69$ GPa, $E^{(3)} = 14$ GPa, $\nu^{(1)} = 0{\cdot}3$, $\nu^{(2)} = 0{\cdot}20$, $\nu^{(3)} = 0{\cdot}2$ was treated in Reference 2. The tangential stress $\sigma_{\theta\theta}$ was evaluated at $R_1' = 40{\cdot}05$ mm, $R_2' = 50{\cdot}05$ mm, $R_3' = 70{\cdot}05$ mm, i.e. very close to the interfaces. A comparison of our analytical results with their numerical ones is shown in Table I.

It should be noted that the FE mesh within the cement and steel layers involved only one element for the whole width of each layer, which presumably was not enough to encapsulate the

Table I. Comparison between analytical and finite element result

Angle	Radius	$\sigma_{\theta\theta}$ (MPa)	
		Analytical	Numerical
0°	R_3'	−19·3	−21
	R_2'	−52·1	−56
	R_1'	−249	−255
60°	R_3'	−21·9	−21
	R_2'	−35·9	−33
	R_1'	−50·2	−52
90°	R_3'	−22·7	−21
	R_2'	−30·4	−29
	R_1'	16·1	27

stress variation within these circular rings. This is likely to be the reason for the great discrepancy observed near the open hole perimeter, at $\theta = 90^\circ$, where a tensile stress is generated.

4. RESULTS

In our computations, we used: $R_3 = 17{\cdot}8$ cm, $R_2 = 14{\cdot}0$ cm, $R_1 = 12{\cdot}7$ cm, $E^{(2)} = 10$ GPa, $E^{(12)} = 200$ GPa, $\nu^{(3)} = 0{\cdot}2$, $\nu^{(2)} = 0{\cdot}2$, $\nu^{(1)} = 0{\cdot}27$, $\sigma_2 = -40$ MPa, $\sigma_1 = -30$ MPa, $\sigma_{r3}^{\infty} = 1$ MPa, $\sigma_{\theta 3}^{\infty} = 3$ MPa. The elasticity moduli for the rock were either $E^{(3)} = 2$ GPa or $E^{(3)} = 20$ GPa, according to the information included in the figure captions. The pressure was either $p = -40$ MPa, $p = -30$ MPa or $p = -20$ MPa as indicated in the labels within the figures.

In Figure 2 we can see the variation of the normalized tangential stress $\sigma_{\theta\theta}$ with the normalized distance r from the edge of the hole, for various pressures p below and above σ_1. The lower the pressure p, the more negative (compressive) the $\sigma_{\theta\theta}$, as expected. The discontinuities occur at the steel/cement and cement/rock interfaces, since continuity for $\sigma_{\theta\theta}$ is not necessarily a consequence of the welded boundary conditions (6) and (8), along these interfaces.

In Figure 3, the variation of the normalized radial stress σ_{rr} with r is presented. Kinks are observed at the interfaces, but continuity is maintained, as required by the boundary conditions (6) and (8).

The in-plane shear stress $\sigma_{r\theta}$ is zero along the x-axis due to the symmetry of the problem.

The change of the anti-plane stresses σ_{r3} and $\sigma_{\theta 3}$, with varying r, is shown in Figures 4 and 5 respectively. While σ_{r3} follows a similar trend with σ_{rr}, $\sigma_{\theta 3}$ decreases, in absolute value, within the steel, while $\sigma_{\theta\theta}$ (Figure 2) increases in absolute value, in that region.

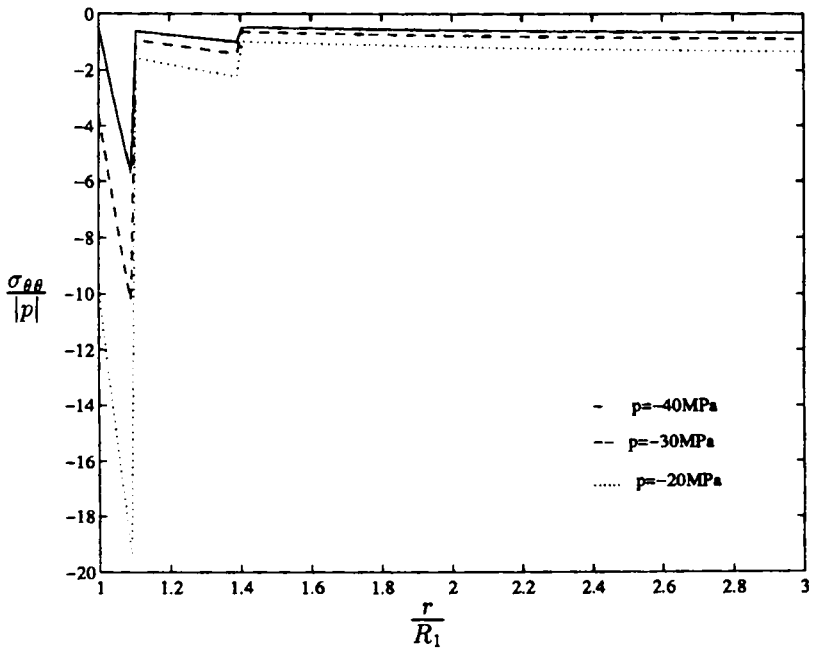

Figure 2. Variation of the normalized tangential stress versus the normalized distance from the borehole centre. $\theta = 0^\circ$, $E^{(3)} = 2$ GPa

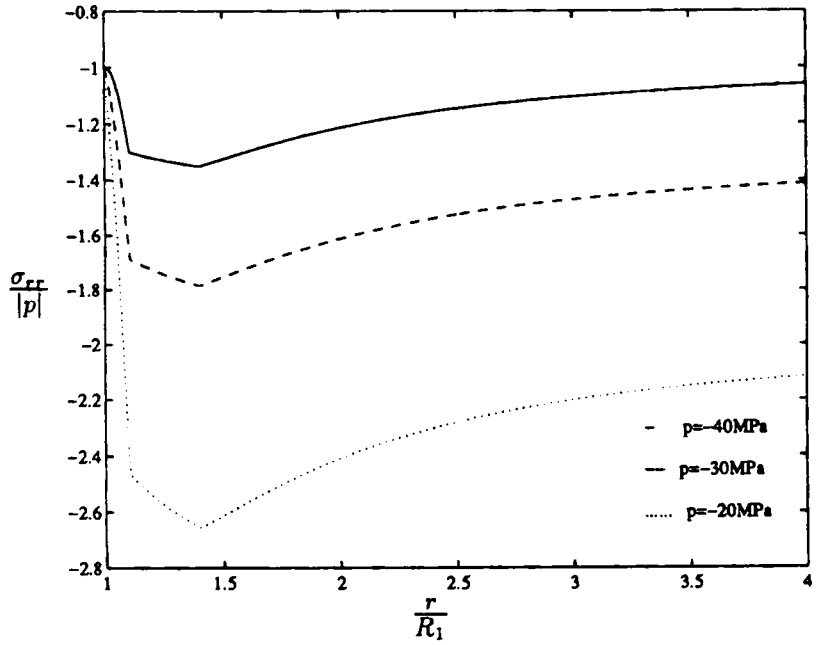

Figure 3. Variation of the normalized radial stress versus the normalized distance from the borehole centre. $\theta = 0°$, $E^{(3)} = 2\,\text{GPa}$

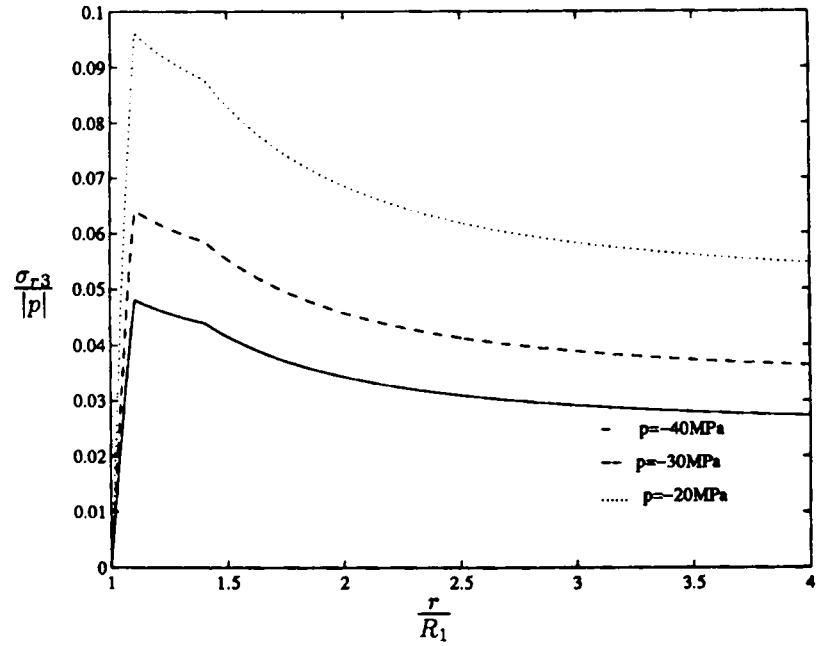

Figure 4. Variation of the normalized anti-plane stress σ_{r3} versus the normalized distance from the borehole centre. $\theta = 0°$, $E^{(3)} = 2\,\text{GPa}$

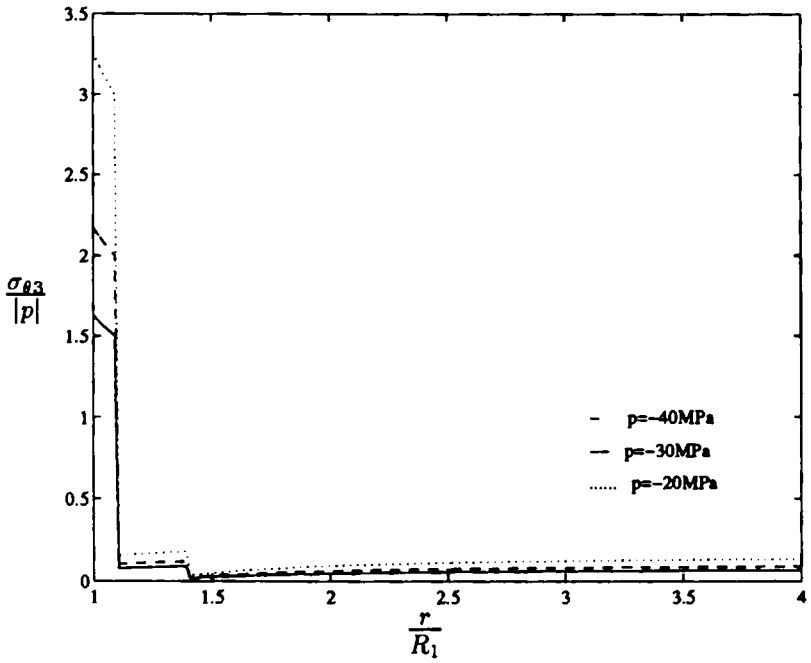

Figure 5. Variation of the normalized anti-plane stress σ_{r3} versus the normalized distance from the borehole centre. $\theta = 0°$, $E^{(3)} = 2$ GPa

The angular variations of the stresses along the interfaces $r = R_1$, $r = R_2$ and $r = R_3$ are depicted in the rest of our graphs. It should be made clear that as far as the (discontinuous along the interfaces) stresses $\sigma_{\theta\theta}$ and $\sigma_{\theta 3}$ are concerned, their evaluation was achieved by using the complex potentials in the region exterior to the circular boundary. Thus for the evaluation of these stresses along $r = R_3$, $\Phi^{(3)}(z)$ nd $\Psi^{(3)}(z)$ were used. Similarly, in the computations performed along $r = R_2$, $\Phi^{(2)}(z)$ and $\Psi^{(2)}(z)$ were implemented.

The fluctuation of the normalized tangential stress versus the angle θ, along the borehole edge, the steel–cement interface and the cement–rock interface, are shown in Figures 6 and 7 respectively. It is worth noting that the maximum (least compressive) stress $\sigma_{\theta\theta}$ occurs at $\theta = 0°$ along the steel–cement boundary, while the maximum $\sigma_{\theta\theta}$ occurs at $\theta = 90°$ along the cement–rock interface. Hence, there is a 90° rotation of the plane of the maximum $\sigma_{\theta\theta}$ between $r = R_2$ and $r = R_3$, which may be an important factor in the initiation and propagation of hydraulic fracture. This observation is discussed further and related to a result from an 'equivalent' inclusion problem, in Section 5.

The angular variation of the in-plane shear stress $\sigma_{r\theta}$ is shown in Figure 8.

In Figures 9 and 10 the angular variation of the normalized anti-plane stress $\sigma_{\theta 3}$, along $r = R_1$, $r = R_2$ and $r = R_3$, is shown. No symmetry is now observed, with respect to the y-axis , because there is not such a symmetry in the loading. On the contrary, there is anti-symmetry with respect to the origin, due to the far field anti-plane loading.

Figures 11–15 show the angular change of the normalized tangential, in-plane shear and anti-plane shear $\sigma_{\theta 3}$ stresses, for $E^{(3)} = 20{,}000$ MPa. In Figure 11, $\sigma_{\theta\theta}$ follows a trend similar to the one shown in Figure 6, but now is less compressive. Figure 12 shows that the maximum tangential stress occurs at $\theta = 0$, along both $r = R_2$ and $r = R_3$, in contrast with Figure 7. This

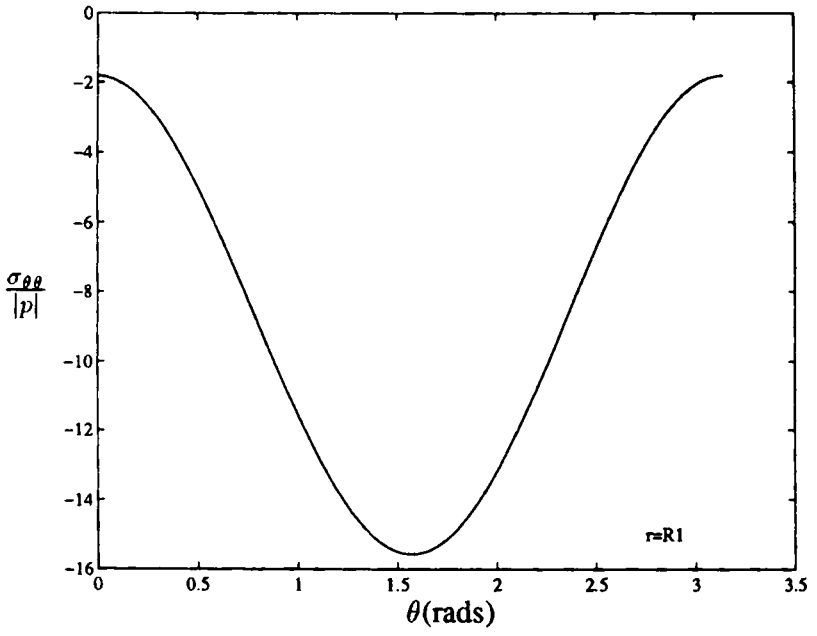

Figure 6. Variation of the normalized tangential stress $\sigma_{\theta\theta}$ versus the angle θ. $E^{(3)} = 2$ GPa

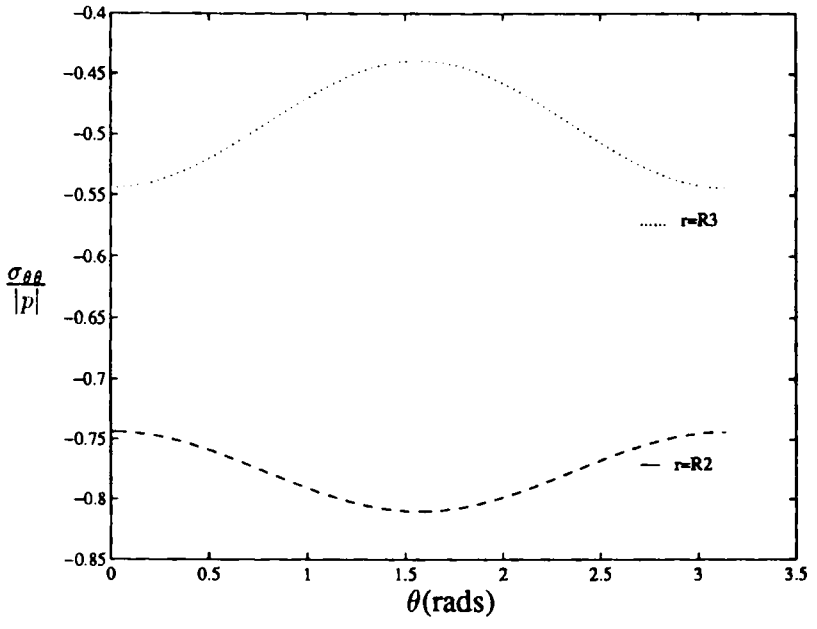

Figure 7. Variation of the normalized tangential stress $\sigma_{\theta\theta}$ versus the angle θ. $E^{(3)} = 2$ GPa

observation is verified by the 'equivalent' inclusion results shown in Table II. The in-plane shear stress in Figure 13 follows a trend similar to the one shown in Figure 8, though having now smaller absolute values.

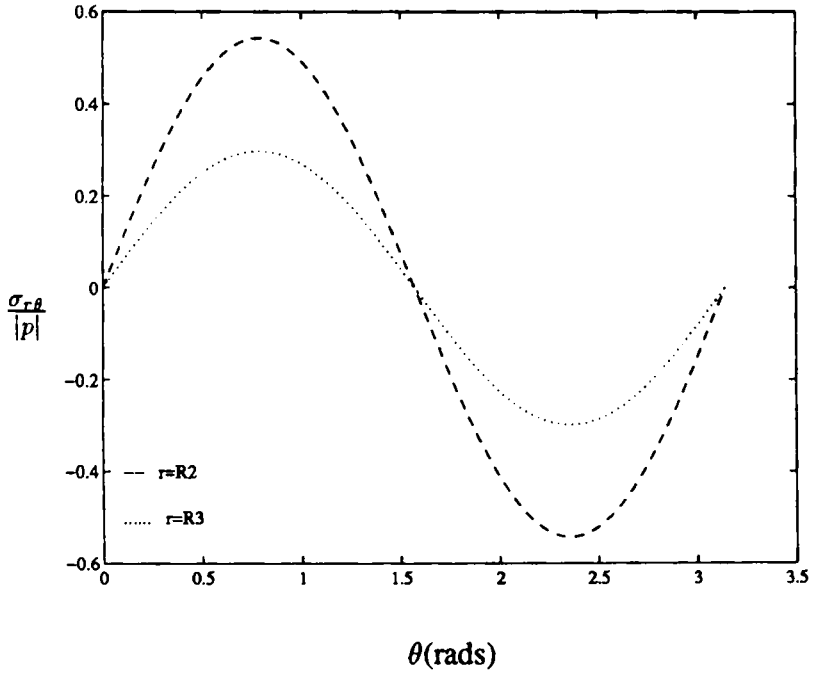

Figure 8. Variation of the normalized in-plane shear stress $\sigma_{r\theta}$ versus the angle θ. $E^{(3)} = 2$ GPa

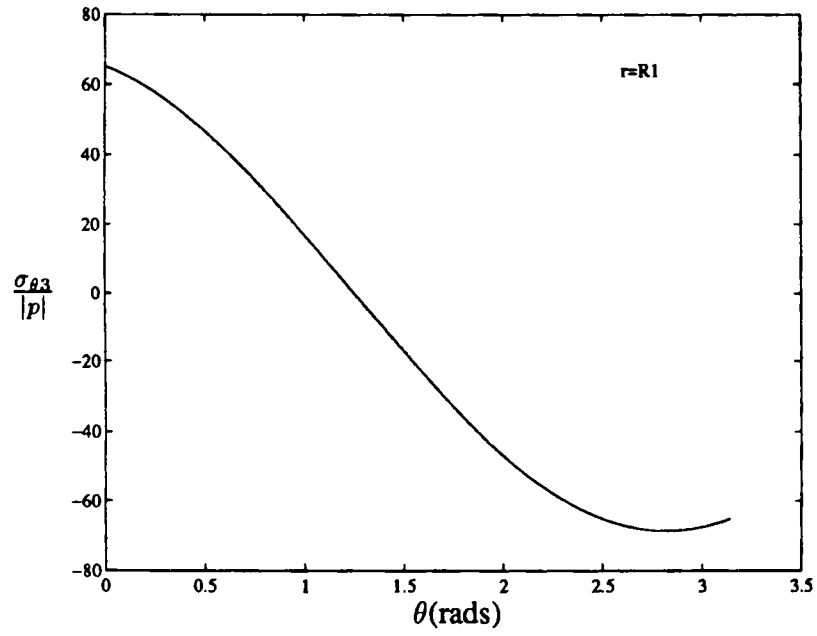

Figure 9. Variation of the normalized anti-plane stress $\sigma_{\theta 3}$ versus the angle θ. $E^{(3)} = 2$ GPa

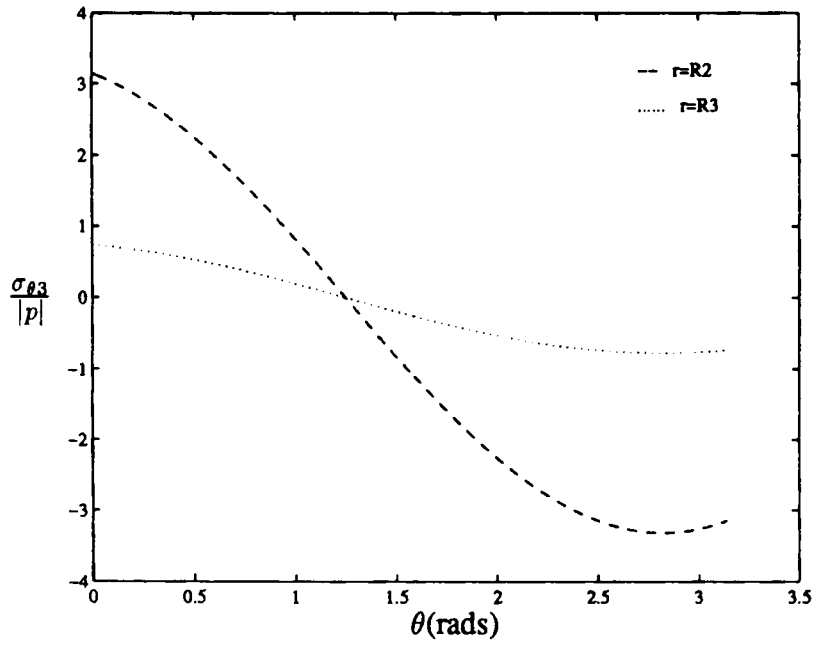

Figure 10. Variation of the normalized anti-plane stress $\sigma_{\theta 3}$ versus the angle θ. $E^{(3)} = 2\,\text{GPa}$

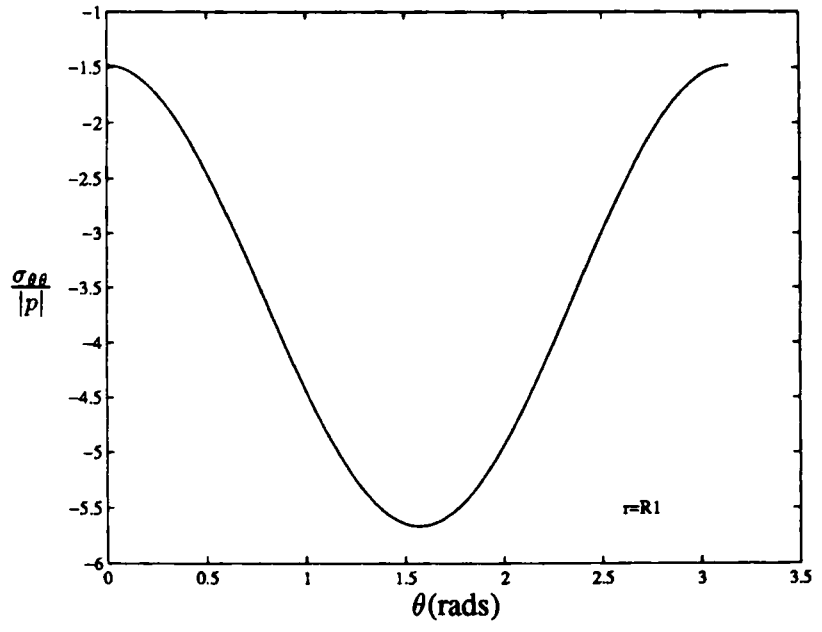

Figure 11. Variation of the normalized tangential stress $\sigma_{\theta\theta}$ versus the angle θ. $E^{(3)} = 20{,}000\,\text{MPa}$

Analogous re-marks can be made for the anti-plane shear stress $\sigma_{\theta 3}$ along $r = R_1$, the variation of which is shown in Figure 14.

It is also worth commenting that, in Figure 15, the values of $\sigma_{\theta 3}$ follow an increasing (in absolute value) trend between $r = R_2$ and $r = R_3$, while $\sigma_{\theta 3}$ in Figure 10 decreases (in absolute

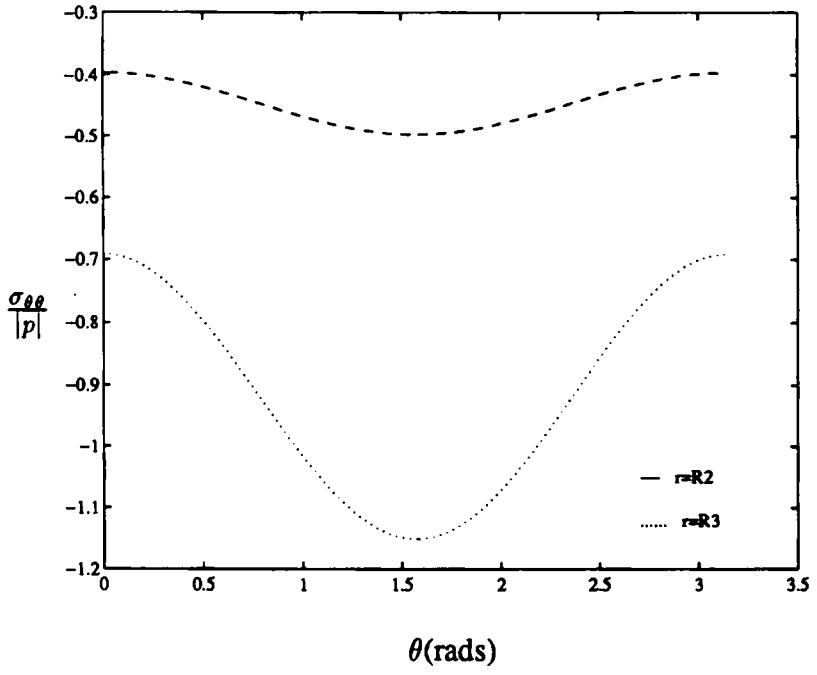

Figure 12. Variation of the normalized tangential stress $\sigma_{\theta\theta}$ versus the angle θ. $E^{(3)} = 20{,}000$ MPa

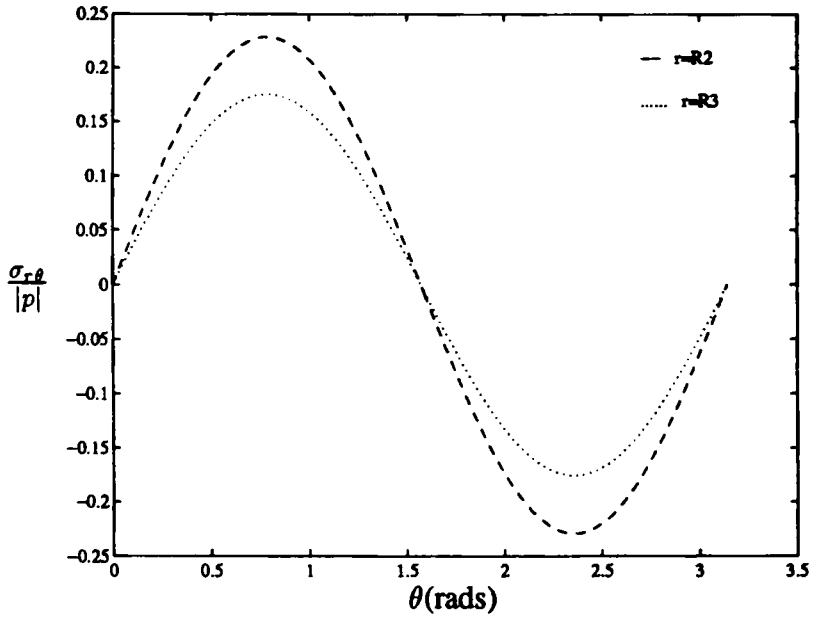

Figure 13. Variation of the normalized in-plane shear stress $\sigma_{r\theta}$ versus the angle θ. $E^{(3)} = 20{,}000$ MPa

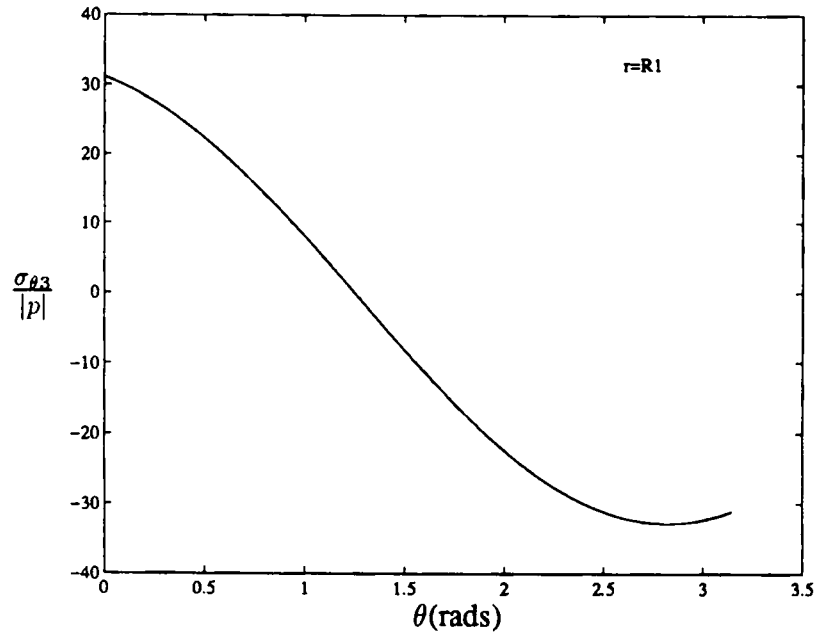

Figure 14. Variation of the normalized anti-plane stress $\sigma_{\theta 3}$ versus the angle θ. $E^{(3)} = 20{,}000$ MPa

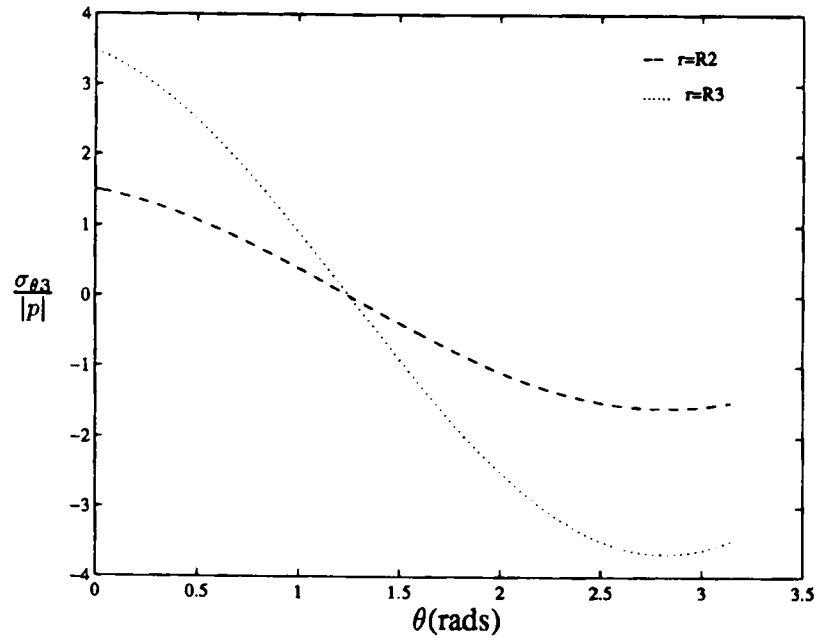

Figure 15 Variation of the normalized anti-plane stress $\sigma_{\theta 3}$ versus the angle θ. $E^{(3)} = 20{,}000$ MPa

value) between $r = R_2$ and $r = R_3$. The same remark can be made for the values of $\sigma_{\theta\theta}$ in Figures 12 and 7 respectively.

As a general comment, it should be mentioned that the effect of the earth stress field, the fluid loading inside the wellbore, the steel casing and the cement annuli can be represented to a suitable

approximation by the boundary value problem treated here. The problem as stated is equivalent to that treated via finite elements Reference 2. In actual engineering practice, the stress evolution as the cement sets, the nature of the cementing process, the poroelastic nature of the rock, the damage effected during drilling and other complications are all likely to require a modification of the problem analysed here. We hope to incorporate some of these features into future work; the present work should be viewed as a first step towards the problem faced in drilling engineering practice.

5. AN 'EQUIVALENT' INCLUSION PROBLEM

As a check on the validity of the observation, regarding the rotation of the plane where the maximum $\sigma_{\theta\theta}$ occurs along the cement–rock interface (see Figure 7), we considered the problem of a circular inclusion, of radius R_3, perfectly bonded to a matrix of different material. Such a solution exists in the literature, but can also be obtained from our analysis, by enforcing that there are no singularities within the inclusion, i.e. $B^{(2)} = 0$, $F^{(2)} = 0$ and $G^{(2)} = 0$. It also turns out that $C^{(2)} = 0$ and from (28), (30) the stress field within the inclusion emerges as uniform, i.e. independent of r. The field functions and the appropriate constants can be found in Appendix III.

We replace the steel layer, the cement layer and the hole in our layered problem by an 'equivalent' inclusion, with shear modulus μ^* given by

$$\mu^* = \frac{(R_2^2 - R_1^2)\mu^{(1)} + (R_3^2 - R_2^2)\mu^{(2)}}{R_3^2} \tag{62}$$

The angle θ, where the maximum $\sigma_{\theta\theta}$ along $r = R_3$ occurs, in the case of this equivalent inclusion problem, is then calculated by using the complex potentials of the matrix and by differentiating $\sigma_{\theta\theta}$ with respect to θ. It was found to be

$$\theta = 0 \quad \text{for} \quad V = \frac{\mu^{(3)} - \mu^*}{\mu^* \kappa^{(3)} + \mu^{(3)}} > -\tfrac{1}{3} \tag{63}$$

$$\theta = \frac{\pi}{2} \quad \text{for} \quad V = \frac{\mu^{(3)} - \mu^*}{\mu^* \kappa^{(3)} + \mu^{(3)}} < -\tfrac{1}{3} \tag{64}$$

Hence the position of the plane of the maximum $\sigma_{\theta\theta}$ depends on the material moduli of steel, cement and rock and the radii of the open hole, the steel/cement interface and the cement/rock interface. The angle θ where the maximum $\sigma_{\theta\theta}$ occurs along $r = R_3$, obtained from the computation for our original problem, is presented in Table II, along with the value of V obtained from the 'equivalent' inclusion analysis, for several values of $E^{(3)}$. It is observed that the 'equivalent' inclusion prediction, from (63) and (64), coincides with the outcome of the computation, except when $V = -0{\cdot}338$, $V \simeq -0{\cdot}342$ and $V = -0{\cdot}347$, i.e. when the relative difference between the minimum and the maximum stress is very small (0.8, 2.2 and 3.9 per cent). This is not too surprising, since the position of the maximum depends on whether V is greater or less than $-\frac{1}{3}$. We would not also expect our 'equivalent' inclusion approximation to exactly mirror the detailed calculations in the sensitive region where V is very close to $-\frac{1}{3}$. Nevertheless, a test of the value of V, provided this value is not too close to $-\frac{1}{3}$, could be used as a rule of thumb for the prediction of the favourable plane of the maximum hoop stress.

As far as the hoop stress along $r = R_3$, evaluated from the field within the equivalent inclusion, is concerned, it was shown that its maximum always occur at $\theta = 0$. This observation does not coincide with the outcome from the computation, which showed that the maximum $\sigma_{\theta\theta}$ occurs at both 0 or $\pi/2$ with varying θ. We note here that we should not expect to compare the field inside

Table II. The angle θ of the maximum $\sigma_{\theta\theta}^{(3)}$ along $r = R_3$, obtained from the original problem computation, along with the equivalent inclusion ratio

$E^{(3)}$ (MPa)	V	θ	$\left[\frac{\sigma_{\theta\theta}^{\min} - \sigma_{\theta\theta}^{\max}}{\sigma_{\theta\theta}^{\max}}\right]$ (%)
50,000	0·245	0	97
20,000	− 0·006	0	66
10,000	− 0·227	0	35
5000	− 0·331	0	6·1
4700	− 0·338	0	3·9
4500	− 0·342	0	2·2
4300	− 0·347	0	0·8
4000	− 0·354	$\pi/2$	1·8
3000	− 0·378	$\pi/2$	10
2000	− 0·403	$\pi/2$	19

the 'equivalent' inclusion with that of the annular composite (hole + steel + cement), since the equivalent inclusion smooths out the stress field. Nevertheless, as we see above, in the region exterior to the cement/rock interface, the 'equivalent' inclusion problem is very accurate.

ACKNOWLEDGEMENTS

Dr. D. A. Eftaxiopoulous gratefully acknowledge the financial support of the European Union, via the Human Capital and Mobility individual fellowship entitled ' Hydraulic fracture propagation from inclined wellbore' (contract ERBCHBICT941080).

APPENDIX I

Definition of constants used in the plane analysis

$$H^{(3)} = A^{(3)} - \frac{F^{(3)}}{R_3^2} \tag{65}$$

$$I^{(3)} = -R_3^2 D^{(3)} \tag{66}$$

$$J^{(3)} = \frac{3B^{(3)}}{R_3^4} - \frac{G^{(3)}}{R_3^6} \tag{67}$$

For $l = 2, 1$, with step -1

$$A^{(l)} = Y_1^{(l,l+1)} A^{(l+1)} + Y_2^{(l,l+1)} H^{(l+1)} \tag{68}$$

$$B^{(l)} = Y_1^{(l,l+1)} B^{(l+1)} + Y_2^{(l,l+1)} I^{(l+1)} \tag{69}$$

$$C^{(l)} = Y_1^{(l,l+1)} C^{(l+1)} + Y_2^{(l,l+1)} J^{(l+1)} \tag{70}$$

$$K^{(l)} = Y_3^{(l,l+1)} A^{(l+1)} + Y_4^{(l,l+1)} H^{(l+1)} \tag{71}$$

$$L^{(l)} = Y_3^{(l,l+1)} B^{(l+1)} + Y_4^{(l,l+1)} I^{(l+1)} \tag{72}$$

$$M^{(l)} = Y_3^{(l,l+1)} C^{(l+1)} + Y_4^{(l,l+1)} J^{(l+1)} \tag{73}$$

$$Y_1^{(l,l+1)} = \frac{\mu^{(l)}\kappa^{(l+1)}}{\mu^{(l+1)}\kappa^{(l)}} + \frac{Y_3^{(l,l+1)}}{\kappa^{(l)}} \tag{74}$$

$$Y_2^{(l,l+1)} = -\frac{\mu^{(l)}}{\mu^{(l+1)}\kappa^{(l)}} + \frac{Y_4^{(l,l+1)}}{\kappa^{(l)}} \tag{75}$$

$$Y_3^{(l,l+1)} = \frac{Y_5^{(l,l+1)}}{\Lambda^{(l)}} \tag{76}$$

$$Y_4^{(l,l+1)} = \frac{Y_6^{(l,l+1)}}{\Lambda^{(l)}} \tag{77}$$

$$Y_5^{(l,l+1)} = -\frac{\mu^{(l)}}{\mu^{(l+1)}}\kappa^{(l+1)} + \kappa^{(l)} \tag{78}$$

$$Y_6^{(l,l+1)} = \frac{\mu^{(l)}}{\mu^{(l+1)}} + \kappa^{(l)} \tag{79}$$

$$\Lambda^{(l)} = \kappa^{(l)} + 1 \tag{80}$$

$$D^{(l)} = -R_{l+1}^2 C^{(l)} - \frac{L^{(l)}}{R_{l+1}^2} \tag{81}$$

$$F^{(l)} = R_{l+1}^2 [A^{(l)} - K^{(l)}] \tag{82}$$

$$G^{(l)} = 3R_{l+1}^2 B^{(l)} - R_{l+1}^6 M^{(l)} \tag{83}$$

$$H^{(l)} = A^{(l)} - \frac{F^{(l)}}{R_l^2} \tag{84}$$

$$I^{(l)} = -R_l^4 C^{(l)} - R_l^2 D^{(l)} \tag{85}$$

$$J^{(l)} = \frac{3B^{(l)}}{R_l^4} - \frac{G^{(l)}}{R_l^6} \tag{86}$$

Also

$$Q_1 = 2Y_1^{(1,2)} + \frac{R_2^2}{R_1^2}[Y_3^{(1,2)} - Y_1^{(1,2)}] \tag{87}$$

$$Q_2 = 2Y_2^{(1,2)} + \frac{R_2^2}{R_1^2}[Y_4^{(1,2)} - Y_2^{(1,2)}] \tag{88}$$

$$Q_3 = Q_1 + Q_2\left[1 - \frac{R_3^2}{R_2^2}\right] \tag{89}$$

$$Q_4 = Q_2\frac{R_3^2}{R_2^2} \tag{90}$$

$$Q_5 = Q_3[Y_1^{(2,3)} + Y_2^{(2,3)}] + Q_4[Y_3^{(2,3)} + Y_4^{(2,3)}] \tag{91}$$

$$Q_6 = -\frac{Q_3 Y_2^{(2,3)} + Q_4 Y_4^{(2,3)}}{R_3^2} \tag{92}$$

$$S_1 = Y_1^{(1,2)} - \frac{3R_1^4 Y_2^{(1,2)}}{R_2^4} + \frac{3R_1^4 R_3^2 Y_2^{(1,2)}}{R_2^6} + \frac{3R_1^2 Y_2^{(1,2)}}{R_2^2} - \frac{3R_1^2 R_3^2 Y_2^{(1,2)}}{R_2^4} + \frac{R_1^2 Y_3^{(1,2)}}{R_2^2} \tag{93}$$

$$S_2 = -Y_2^{(1,2)} R_2^4 + R_2^2 R_3^2 Y_2^{(1,2)} - R_1^4 Y_1^{(1,2)} + R_1^2 R_2^2 Y_1^{(1,2)} - R_1^2 R_2^2 Y_4^{(1,2)} + R_1^2 R_3^2 Y_4^{(1,2)} \tag{94}$$

$$S_3 = \frac{R_2^2 Y_2^{(1,2)} + R_1^2 Y_4^{(1,2)}}{R_3^2} \tag{95}$$

$$S_4 = -\frac{R_1^4 R_3^6 Y_2^{(1,2)}}{R_2^6} + \frac{R_1^2 R_3^6 Y_2^{(1,2)}}{R_2^4} \tag{96}$$

$$S_5 = S_3 Y_3^{(2,3)} + S_1 Y_1^{(2,3)} + \frac{3[S_4 Y_4^{(2,3)} + S_2 Y_2^{(2,3)}]}{R_3^4} \tag{97}$$

$$S_6 = -\frac{S_4 Y_4^{(2,3)} + S_2 Y_2^{(2,3)}}{R_3^6} \tag{98}$$

$$S_7 = -R_3^2 [S_3 Y_4^{(2,3)} + S_1 Y_2^{(2,3)}] \tag{99}$$

$$T_1 = \frac{3Y_2^{(1,2)}}{R_2^4} - \frac{3R_3^2 Y_2^{(1,2)}}{R_2^6} + \frac{3Y_1^{(1,2)}}{R_1^4} - \frac{3R_2^2 Y_1^{(1,2)}}{R_1^6} + \frac{3R_2^2 Y_4^{(1,2)}}{R_1^6} - \frac{3R_3^2 Y_4^{(1,2)}}{R_1^6} \tag{100}$$

$$T_2 = Y_1^{(1,2)} - \frac{3R_2^4 Y_2^{(1,2)}}{R_1^4} + \frac{3R_2^2 R_3^2 Y_2^{(1,2)}}{R_1^4} + \frac{3R_2^6 Y_2^{(1,2)}}{R_1^6} - \frac{3R_2^4 R_3^2 Y_2^{(1,2)}}{R_1^6} + \frac{R_2^6 Y_3^{(1,2)}}{R_1^6} \tag{101}$$

$$T_3 = \frac{3R_2^2 Y_2^{(1,2)}}{R_1^4 R_3^2} - \frac{3R_2^4 Y_2^{(1,2)}}{R_1^6 R_3^2} \tag{102}$$

$$T_4 = \frac{R_3^6 Y_2^{(1,2)}}{R_2^6} + \frac{R_3^6 Y_4^{(1,2)}}{R_1^6} \tag{103}$$

$$T_5 = T_1 Y_1^{(2,3)} + T_3 Y_3^{(2,3)} + \frac{3[T_2 Y_2^{(2,3)} + T_4 Y_4^{(2,3)}]}{R_3^4} \tag{104}$$

$$T_6 = -\frac{T_4 Y_4^{(2,3)} + T_2 Y_2^{(2,3)}}{R_3^6} \tag{105}$$

$$T_7 = -R_3^2 [T_1 Y_2^{(2,3)} + T_3 Y_4^{(2,3)}] \tag{106}$$

APPENDIX II

Definition of constants used in the anti-plane analysis

For $l = 1, 2$

$$Y_1^{(l,l+1)} = \frac{1}{2}\left[1 + \frac{\mu^{(l)}}{\mu^{(l+1)}}\right] \tag{107}$$

$$Y_2^{(l,l+1)} = \frac{1}{2}\left[1 - \frac{\mu^{(l)}}{\mu^{(l+1)}}\right] \tag{108}$$

$$A^{(l)} = Y_1^{(l,l+1)} A^{(l+1)} + Y_2^{(l,l+1)} \frac{B^{(l+1)}}{R_{l+1}^2} \tag{109}$$

$$B^{(l)} = Y_1^{(l,l+1)} B^{(l+1)} + Y_2^{(l,l+1)} R_{l+1}^2 A^{(l+1)} \tag{110}$$

and

$$Y_5 = Y_3 Y_1^{(2,3)} + Y_4 Y_2^{(2,3)} R_3^2 \tag{111}$$

$$Y_6 = Y_3 \frac{Y_2^{(2,3)}}{R_3^2} + Y_4 Y_1^{(2,3)} \tag{112}$$

$$Y_3 = \frac{Y_1^{(1,2)}}{R_1} + Y_2^{(1,2)} \frac{R_2^2}{R_1^3} \tag{113}$$

$$Y_4 = \frac{Y_2^{(1,2)}}{R_2^2 R_1} + \frac{Y_1^{(1,2)}}{R_1^3} \tag{114}$$

APPENDIX III

Field constants for the equivalent inclusion problem

The field constants for the equivalent inclusion and the matrix are superscripted by (2) and (3) respectively. Their names and the algebraic expressions for the field functions are the same as the ones corresponding to the rock and cement in Section 1.

$A^{(3)}$ and $D^{(3)}$ are given from (13) and (14).

$$B^{(3)} = \frac{Y_2^{(2,3)} R_3^2 D^{(3)}}{Y_1^{(2,3)}} \tag{115}$$

$$F^{(3)} = \frac{R_3^2 [- Y_1^{(2,3)} - Y_2^{(2,3)} + Y_3^{(2,3)} + Y_4^{(2,3)}] A^{(3)}}{- Y_2^{(2,3)} + Y_4^{(2,3)}} \tag{116}$$

$$G^{(3)} = \frac{3 R_3^4 Y_2^{(2,3)} D^{(3)}}{Y_1^{(2,3)}} \tag{117}$$

$$A^{(2)} = Y_1^{(2,3)} A^{(3)} + Y_2^{(2,3)} \left[A^{(3)} - \frac{F^{(3)}}{R_3^2} \right] \tag{118}$$

$$B^{(2)} = C^{(2)} = F^{(2)} = G^{(2)} = 0 \tag{119}$$

REFERENCES

1. J. L. Carvalho, 'Stability of deviated boreholes', *Dowell Schlumberger Report, DL 10377*, August 1988.
2. B. J. Carter, P. A. Wawrzynek and A. R. Ingraffea, 'Effects of casing and interface behavior in hydraulic fracture', in H. J. Siriwardane and M. M. Zaman (eds), *Proc. 8th Int. Conf. on Computer Methods and Advances in Geomechanics*, Morgantown, West Virginia, U.S.A., 22–28 May 1994, Balkema, Rotterdam, 1994.
3. N. I. Muskhelishvili, *Some Basic Problem of Mathematical Theory of Elasticity*, Nordhoff International Publishing, Leyden, 1977.
4. D. R. List, 'A two dimensional circular inclusion problem', *Proc. Cambridge Philos. Soc.*, **65**, 823–830 (1969).